On the Bimodal Effects of Silicic Acids on Calcite Growth

Carlos M. Pina,*,† Casjen Merkel,‡ and Guntram Jordan‡

† Department of Crystallography and Mineralogy, Complutense University of Madrid, 28040 Madrid, Spain, and ‡Department für Geo- und Umweltwissenschaften, Ludwig-Maximilians-Universitat, 80333 Munchen, Germany

ABSTRACT: The effects of silicic acids on calcite growth are a model for the effects of partially polymerized additives on crystal growth. At alkaline pH, silicic acid polymers coexist with small mono- and oligomers. Atomic force microscopy (AFM) showed that large polymers promote two-dimensional nucleation, while mono- and oligomers have a bimodal promoter/inhibitor effect on step propagation. This bimodality can be interpreted as the result of attachment of mono- and oligomers along the steps along with a modification of the kinetics of kink generation and/or propagation. The bimodal step kinematic effect is accompanied by a single morphologic effect: growth islands transform from a rhombus into an ellipse. This effect has been reported for other additives, indicating that many additives generate few morphologies. Such a convergence limits the versatility of chemical control on biomorphogenesis. Contrarily, the strong kinetic effect of silicic acids may make them very efficient controllers of biomorphogenesis, if coupled with a physical shape control, for example, by templates. Thus, silicic acids show a unique bimodality as a controller of calcite biomineralisation and as an abundant biomineral.

Introduction

Organisms show amazing capabilities to control crystal morphologies. These capabilities have drawn close attention of not just biologists but also of material scientists and geochemists.[1,2] In this context, intense research is focusing on the molecular mechanisms of this morphology control. The discussed mechanisms can be divided into two groups: physically and chemically controlled.[3] In order to investigate the latter, effects of various different additives have been studied on calcite surfaces. The additives used range from divalent metal cations,[4-6] via anionic ligands such as oxalate, aspartate, EDTA[7,8] to large polymer molecules such as proteins or polysaccarides.[9-11]

However, although there is a huge number of additives, the number of types of calcite habits and morphologies generated by the additives is rather limited, for example, spherulites, dumbbell-like and rounded morphologies, blocky crystals, and crystals with vicinal faces.[6,12] On the calcite (104) surface, AFM studies yielded an even more limited number of different features: essentially, only straight steps which form angles with the ⟨441⟩ and ⟨481⟩ main step directions as well as curved and rough steps were obtained.[13-16]

The AFM studies have further shown that most additives induce a retarded step advance rate or even cause the growth to cease completely (i.e., the so-called dead zone). Only a few additives such as polypeptides and proteins[9,17,18] have been reported to have a promoting effect on calcite step advance rates which at higher additive concentrations transforms into an inhibiting effect. Growth promotion has been attributed to the so-called thermodynamic effect of additives, that is, to a decrease in interface energy of the growing surface.[19] Such an energy decrease can lead to both a higher kink density along the steps and an increase of the two-dimensional nucleation rate. The concentration of a given growth promoter $C_{p\ max}$ which relates to the maximum growth rate of a given surface is supposed to depend on the supersaturation but in general is thought to be low.19 The reason why so few growth promoters have been reported so far, therefore, might be related to these very small values of Cp max, which also reduce the interface energy only by a very small value, if any.

Promoters reported in the literature generally are ligands such as sulfate[19] or aspartate oligomers[8,17] and proteins.[9] While in the case of sulfate the promotion has been attributed to a solid solution effect causing a modified solubility due to the incorporation of sulfate into the calcite lattice, other additives were related to the above-mentioned thermody-namic effect. Nonincorporating growth promoters found so far are large organic ligands which, if surrounded by the growing crystal, are forming inclusions rather than being incorporated into lattice sites. Additionally, it has been shown that among these additives, the aspartate oligomers and proteins show a positive correlation between the magnitude of the promoting effect and the net charge of the molecule.[8]

On this background, there are a few questions that need to be addressed: Is it an exclusive property of large organic ligands to promote calcite growth via a nonincorporating thermodynamic effect? What is the mechanism of the growth promotion on the calcite surface? Does this mechanism depend on the degree of polymerization of the additives (molecules)? Does the morphogenetic effect of promoters depend on the nature of the additive?

The investigation of the effect of silicate solutions on calcite growth kinetics and morphology might be a good way to address some of these questions because of their nonorganic nature - which does not mean that silica is absent in biological systems[21] - and their ability to form monomeric, oligomeric, and polymeric species with uniform functional groups and anionic charge. At alkaline pH, sodium silicate solutions form partially deprotonated silicic acids (i.e., the monomers $H_3SiO_4^-$ and $H_2SiO_4^{2-}$) which in part polymerize to form oligomers and polymers which might be compared to proteins. The degree of polymerization reveals a pronounced bimodality.[21]

Table 1. Experimental Conditions: Concentrations, pH, and Supersaturation with Respect to Calcite

exp. no.	$[CaCl_2]$ mmol/L	$[Na_2CO_3]$ mmol/L	$[Na_2SiO_3]$ mmol/L	$[Si]_{tot}$ ppm	pH	supersaturation $\beta_{calcite}$
1	0.5	0.5	0	0	10.25	16.6
2	0.5	0.5	0.082	2.3	10.22	16.2
3	0.5	0.5	0.164	4.6	10.17	15.5
4	0.5	0.5	0.246	6.9	10.20	15.9
5	0.5	0.5	0.328	9.2	10.21	15.9
6	0.5	0.5	0.41	11.5	10.21	15.9
7	0.5	0.5	0.615	17.2	10.21	15.5
8	0.5	0.5	0.82	23.2	10.22	15.9
9	0.5	0.5	1.64	45.9	10.21	15.1
10	0.375	0.375	0	0	10.19	10.0
11	0.375	0.375	0.082	2.3	10.24	10.2
12	0.375	0.375	0.123	3.4	10.22	10.2
13	0.375	0.375	0.164	4.6	10.22	10.2
14	0.375	0.375	0.205	5,7	10.19	9.8
15	0.375	0.375	0.246	6.9	10.23	10.2
16	0.375	0.375	0.328	9.2	10.22	10.0
17	0.375	0.375	0.41	11.5	10.23	10.0
18	0.375	0.375	0.615	17.2	10.18	9.6
19	0.375	0.375	0.82	23.2	10.17	9.3
20	0.375	0.375	1.64	45.9	10.27	10.0
21	0.285	0.285	0	0	10.19	6.3
22	0.285	0.285	0.082	2.3	10.21	6.5
23	0.285	0.285	0.164	4.6	10.22	6.5
24	0.285	0.285	0.246	6.9	10.20	6.3
25	0.285	0.285	0.328	9.2	10.21	6.3
26	0.285	0.285	0.41	11.5	10.20	6.3
27	0.285	0.285	0.615	17.2	10.17	6.0
28	0.285	0.285	0.82	23.2	10.21	6.2
29	0.285	0.285	1.64	45.9	10.23	6.0
30	0.1875	0.1875	0	0	10.15	3.0
32	0.1875	0.1875	0.082	2.3	10.16	3.0
33	0.1875	0.1875	0.123	3.4	10.16	3.0
34	0.1875	0.1875	0.164	4.6	10.20	3.1
35	0.1875	0.1875	0.205	5.7	10.18	3.1
36	0.1875	0.1875	0.246	6.9	10.19	3.1
37	0.1875	0.1875	0.328	9.2	10.15	3.0
38	0.1875	0.1875	0.615	17.2	10.18	3.0

This bimodality provides the unique possibility to distinguish between the effects of mono- and oligomers and polymers within a single experiment since the polymers can be recognized by AFM and can be relocated by the AFM tip.

Natural settings may contain up to 600 μM silicic acid. Typical values range from approximately 20-600 μM in fresh water to 10 μM in seawater, whereas soil solutions contain around 0.1-1.5 mM.[23] Therefore, if silicic acids and their polymerizations are capable of promoting calcite growth, the question may become important as to whether natural calcium carbonate crystals with spherule habits and filament habits are a reliable indicator of biological activity. To find an answer to this question is especially important since several authors have recently demonstrated that the presence of dissolved silica in the crystallization medium is related to the formation of fractal and biomorphic-like carbonate crystals and crystalline aggregates.[24-28]

Experimental Procedures

In situ growth experiments were carried out at room temperature in different atomic force microscopes (AFM) equipped with a fluid cell (Multimode, Veeco Instruments; NanoWizard II, JPK Instru-ments). All the images shown in this work were taken in contact mode while displaying both height and deflection signals. Silicon and silicon nitride cantilevers with triangular tips with nominal force constants of 0.02-0.77 N/m were used (Veeco NP). The length of the tips was 200 μm. Optically clear calcite crystals from India were cleaved with a blade razor parallel to (104) immediately before each experiment. Before injecting the growth solutions, deionized water was passed over the calcite surfaces. Characteristic shallow and deep etch pits formed during dissolution. These pits were used to determine the orientation of obtuse and acute monosteps.[29,30] Growth solutions were prepared from reagent grade $CaCl_2$,$NaCO_3$, and $NaSiO_3$ solutions and deionized water (Milli-Q Millipore; resistivity 18 MΩ cm). Prior to each experiment, the pH of the solution was adjusted to 10.20 (0.05 by adding NaOH or HCl. The pH of the solutions was measured with a pH-meter (Crison GLP21) immediately before injecting them into the fluid cell of the AFM. In addition, the adjusted pH of the solutions was checked several times during the experiments. The activities of Ca^{2+}, H_2CO_3, HCO_3^-, CO_3^{2-}, $H_2SiO_4^{2-}$, H_3SiO^{4+}, and H_4SiO_4 in solution were calculated using PHREEQC.[31] The supersaturation of the solutions with respect to calcite was calculated using the following expression:

$$\beta_{calcite} = \frac{a(Ca^{2+})a(CO_3^{2-})}{K_{sp,\,calcite}}$$

where $a(Ca^{2+})$ and $a(CO_3^{2-})$ are the activities of the ions in the solution and $K_{sp,calcite} = 10^{-8.48}$ is the solubility product for calcite at 25 °C. Table 1 shows the concentrations of $CaCl_2$, Na_2SO_4, and Na_2SiO_3, the pH values, and the supersaturations with respect to calcite of the aqueous solutions used in the experiments.

In order to keep the composition in the fluid cell constant, experiments were conducted both with a continuous flow and with a discontinuous fluid injection method. In the latter, fresh solution was injected at intervals of about 1 min between each AFM scan. AFM images were obtained at scan rates which varied from ~4 to 20 Hz and 256 to 512 lines per scan. Maximum scan areas were 14 X 14 μm2. For each supersaturation-silica concentration pair, the growth velocities of the acute and obtuse calcite steps were measured from sequences of AFM deflection images. In order to minimize random errors, several runs of each experiment were conducted and velocities were measured for at least two different steps for each run.

For the high alkalinity of the solutions used in this work, a bimodal distribution of polymerized silicic acids is expected;[22,32] that is, partially deprotonated monomeric and oligomeric silicic acids and large silica polymers with partially deprotonated silanol groups (here called polysilicic acids) coexist in the aqueous solutions. These two groups of silicic acids affect the growth behavior of calcite (104) differently and therefore will be discussed separately.

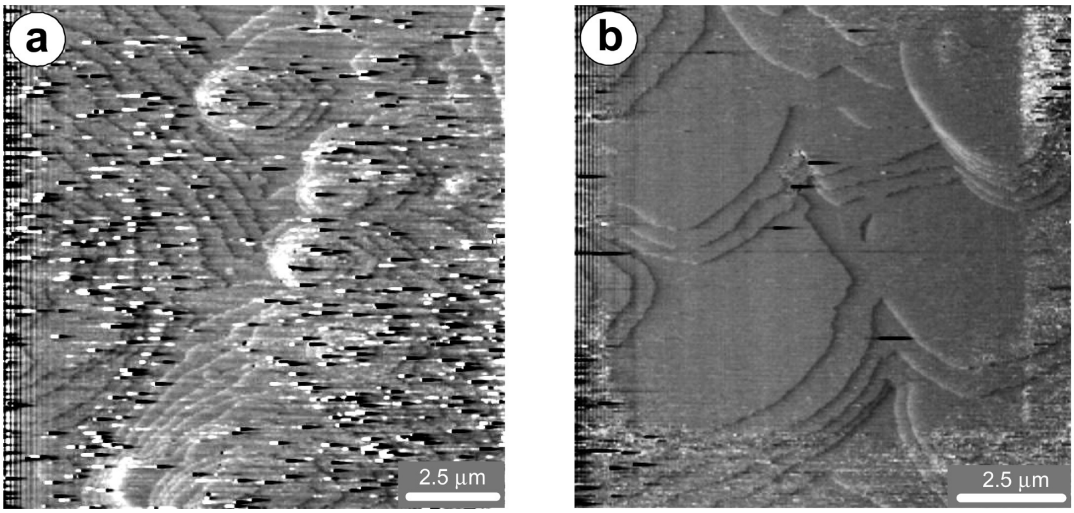

Figure 1. (a) AFM image of large particles attached to the calcite (104) surface. Note that two-dimensional nucleation is related to the particles (solution: $\beta_{calcite} = 10$; $[Si]_{tot} = 6.8$ ppm). (b) AFM image of steps propagating into the scan area from the area outside which has not been cleared from attached particles (solution: $\beta_{calcite} = 10$; $[Si]_{tot} = 2.27$ ppm).

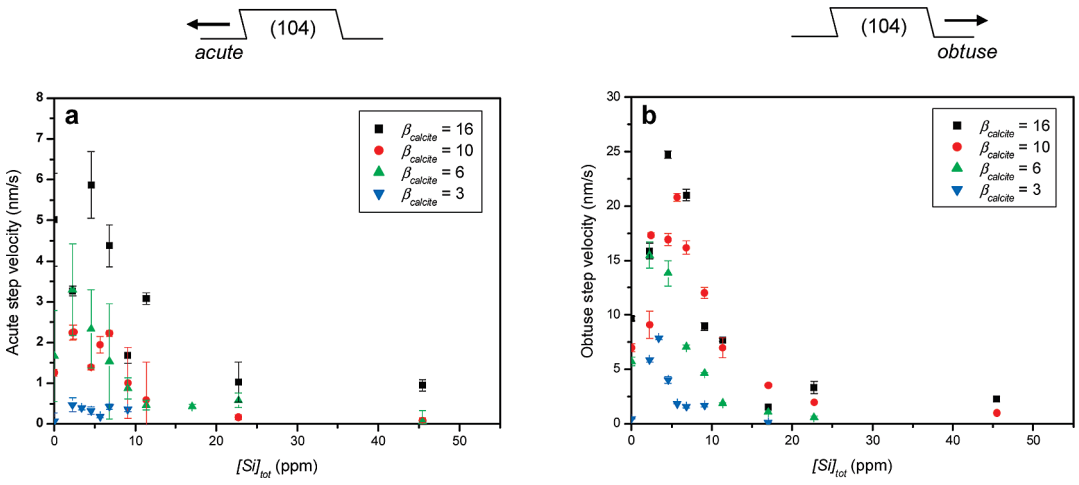

Figure 2. Calcite step velocities as a function of the total Si concentration in the aqueous solution for different supersaturations with respect to calcite: (a) acute steps and (b) obtuse steps. The drawings on the top of the plots illustrate the orientation of the steps with respect to the calcite (104) surface as well as the propagation direction.

Results and Discussion

Effect of Large Polysilicic Acids. Large particles are fre-quently observed on the calcite (104) surface. These particles can be interpreted as polysilicic acids. The particles reach sizes of up to about 50 nm. The polysilicic acids can be removed with the AFM tip while scanning, indicating that they are only weakly attached to the calcite surface. The attachment fre-quency of polysilicic acids is slow enough such that, once a polymer-free scan-field is created by the tip, an almost clear surface can be maintained by applying tip velocities of about 140-280 µm/s without the necessity of any elevated tip loading forces which might influence the step movement. At the remaining silica particles the formation of calcite (104) islands (one calcite monolayer in height) can frequently be observed. Thus, the large polysilicic acid particles strongly promote two-dimensional nucleation (Figure 1a). On particle-free scan-fields two-dimensional nucleation was either signifi-cantly reduced or no nucleation was observed at all. Within these scan-fields steps mainly propagate from the surrounding unscanned area, indicating that an intense two-dimensional nucleation takes place outside of the observation field where the scanning tip is not able to remove large polysilicic acids.(Figure 1b). The promotion of two-dimensional nucleation on the calcite (104) surface by the polysilicic acids can be related to the negatively charged deprotonated silanol groups on the surface of such polymers which likely cause Ca^{2+} from the solution to attach. The reference experiments without silicic acids did show significantly lower nucleation densities on calcite surfaces.

Effect of Mono- and Oligomeric Silicic Acids. AFM-mea-surements of step positions versus time have shown that the concentration of silicic acids in the solution has a complex effect on the step kinematics. Figure 2 shows the depen-dency of step velocities of obtuse and acute calcite steps on total concentration of Si in the range of super-saturations $3<\beta_{calcite}<16$: for all supersaturations studied, the velocities of both obtuse and acute steps increase for $[Si]_{tot}$ below ~5.7 ppm.

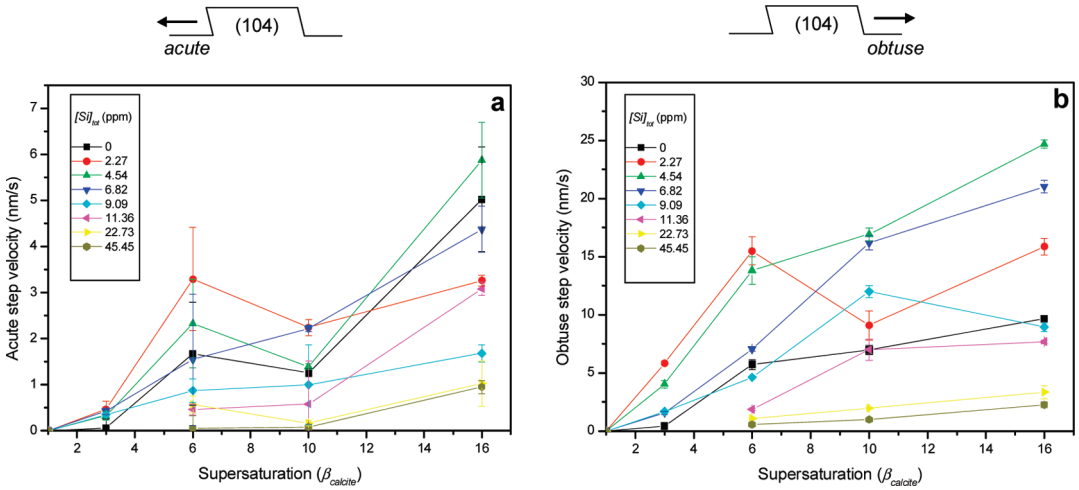

Figure 3. Step velocities versus supersaturation $\beta_{calcite}$ for different total Si concentrations: (a) acute steps and (b) obtuse steps. The drawings on the top of the plots illustrate the orientation of the steps with respect to the calcite (104) surface as well as their propagation direction.

The obtained data of silica concentration with the max-imum step rate $Si_{p\ m\ a\ x}$ do not reveal a significant dependency on the supersaturation. The initial increase in step velocity is followed by a strong decrease for $[Si]_{tot}$>5.7 ppm. For $[Si]_{tot}$> 11.5 ppm, the measured velocities of acute and obtuse steps are lower than 2 and 7 nm/s, respectively. It needs to be noted, however, that both steps do not stop completely in the range of silicic acid concentrations used. That is, the "dead zone" is not reached. Since the measured step velocities are indepen-dent of the presence of large polysilicic acids particles within the scan-field, the observed kinetics must be a function of the mono- and oligomeric species. Unfortunately, they cannot be detected within the AFM-images of the growing calcite surface due to their small size.

The promotion mechanism may be as follows: monomeric and oligomeric silicic acid species attach to the calcite step edges. The attached species attract Ca^{2p} ions and favor their local desolvation, which is considered to be the rate-limiting step in the growth of calcite.[33] Therefore, at low concentra-tions these species promote kink generation and/or kink propagation along the steps. Thus, the kink-density might be enhanced by mono- and oligomeric species in a similar way as large polysilicic acids enhance the density of two-dimensional nuclei on the calcite (104) surface. A precondi-tion to the promotion might be the existence of at least two negatively charged functional groups leaving at least one negatively charged functional group active after the ligand attached to the step edge. Increasing promotion of calcite growth with an increasing number of functional groups has also been reported for solutions containing aspartate.[8] Cal-culations conducted with PHREEQC show that under the high alkalinity of the solutions (pH 10.2 (0.5) the predo-minant monomeric silicic acids are $H_3SiO_4^-$ and $H_2SiO_4^{2-}$, while the activities of other monomeric species are orders of magnitude lower. Since the promotion of step growth may be favored by silicic acid species with at least two negatively charged functional groups, species such as $H_2SiO_4^{2-}$ or $H_4Si_2O_7^{2-}$ might be considered as mainly responsible for such a promotion.

By increasing $[Si]_{tot}$ the number of ligands attached along the calcite step edges also increases. Above a certain con-centration of attached ligands, the density of ligand-free step edge sites falls below a critical value which causes a net reduction of attachment of calcite growth units. A progres-sive inhibition of step advancement occurs and step rates rapidly decrease as a result. Thus, the inhibition mechanism can be perceived as a screening process of calcite step edge sites by silicic acid species. Additionally, not all of them may actually have a promoting effect.

Elhadj et al.[8] have also observed a dual promotion-inhibition effect of aspartate and aspartate-rich peptide additives on calcite step growth. These authors observed that the total inhibition of the step advance occurred at decreasing peptide concentration as the length of the peptide increased. This suggests that the screening of calcite step edge sites requires a number of peptides which is inversely corre-lated to their length. Since $[Si]_{p\ max}$ is almost constant, it can be assumed that the ligands attached to the step edges have a comparable size within the entire range of supersaturations investigated here. In contrast to the reported dead super-saturation zone induced by aspartate and aspartate rich proteins, the silicic acids do not reveal any dead zone at all, although being a bimodal promoter-inhibitor.

Both the absence of a dead zone and the $[Si]_{tot}$-dependent bimodal promoter-inhibitor effect of silicic acids are further evidenced in Figure 3. In this figure, the step velocities have been plotted as a function of supersaturation for the different values of $[Si]_{tot}$. At $[Si]_{tot}$>11.5 ppm obtuse and acute step velocities > 0 lie below the velocities of the Si-free system within the whole range of supersaturation. For $[Si]_{tot}$<11.5 ppm steps velocities are faster than in the Si-free system.

Data as shown in Figure 3 are used to infer the crystal growth inhibition mechanisms, for example, the step pinning model[34] and the impurity incorporation model.[35-37] The step pinning model assumes that impurities attach at step edges forming a fence that completely inhibits the growth below a given supersaturation for which the radius of the two-dimensional nucleus is smaller than half of the distance between the attached impurities. By increasing supersatura-tion, the radius of the two-dimensional nucleus decreases and the growth is progressively recovered. This is reflected in the step rate as a function of supersaturation by an increase in step velocity that approaches the values of the pure system. In contrast, the impurity incorporation model posits that the incorporation of impurity into lattice sites leads to a decrease in the crystal solubility and, therefore, in the effective supersaturation. As a result, the step velocity for a given supersaturation always remains lower than in the pure system, which is attributed to the shift in the thermo-dynamic equilibrium due to the impurity incorporation.[38]

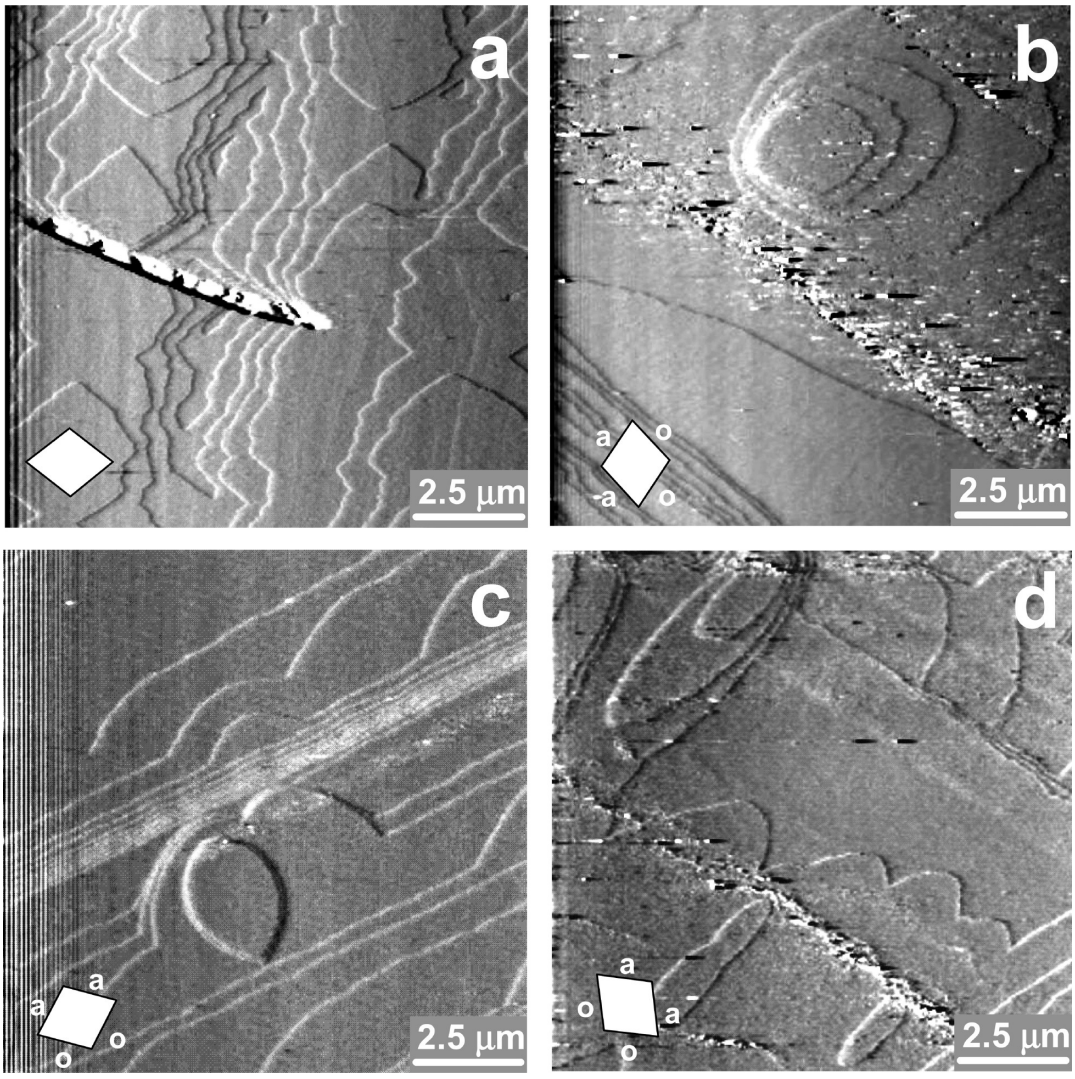

Figure 4. AFM images of calcite (104) surfaces growing at $\beta_{calcite} = 10$ in the presence of increasing concentrations of silicic acids: (a) $[Si]_{tot} = 0$ ppm, (b) $[Si]_{tot} = 3.4$ ppm, (c) $[Si]_{tot} = 5.7$ ppm, and (d) $[Si]_{tot} = 23.2$ ppm. Note that by an increasing rounding of the steps and step junctions, the typical rhombus-shaped islands progressively change into ellipse-shaped islands with the major axis in [$\bar{4}$21]. The orientation of obtuse (o) and acute (a) steps is indicated in the lower left corner of each image.

Obviously, the data presented in Figure 3 do not corre-spond to either of the behaviors described above, indicating that the mono- and oligomeric silicic acids are neither able to effectively pin the steps nor to incorporate into the calcite structure. Thus, the data in Figure 3 indicate that classical models of crystal growth are not adequate to describe the step kinematics affected by additives such as silicic acids with a bimodal promoter/inhibitor effect. Improvements of the models will have to consider that additives may not just be merely blocking or incorporating entities but may be chemi-cal species which can interact with a growing crystal surface in various concentration-dependent ways.

Morphologic Effects of Silicic Acids. In situ AFM observa-tions of the morphology of the growing calcite (104) surface are shown in Figure 4. In Si-free solutions (Figure 4a), two-dimensional islands show their typical rhombus-shape. At low concentrations of silicic acids ($[Si]_{tot} = 3.4$ ppm; Figure 4b), acute and obtuse steps as well as the acute/acute and acute/obtuse step junctions become slightly rounded. With a further increase in the concentration of silicic acids ([Si]tot = 5.7 ppm; Figure 4c) a progressive degree of round-ing can be observed which affects the acute/acute and acute/obtuse step junctions, leaving only one obvious edge at the obtuse/obtuse step junction.

Finally, at a silicic acid concen-tration of $[Si]_{tot} = 23.2$ ppm (Figure 4d) also the obtuse/obtuse junction is affected by the rounding process. The morphology eventually obtained consists of completely rounded islands forming an ellipse with the major axis in [421]. Thus, although there is a pronounced bimodality in the effect of silicic acids on the step kinematics, there is only a single effect on step morphology: the progressive change from a rhomb in $\langle 441 \rangle$ and $\langle 481 \rangle$ to an ellipse with the major axis in [421].

The rounding and elongation reflect a significant change in the anisotropy of step advance which ultimately stems from modified kink generation frequencies (i_o and i_a at obtuse and acute steps, respectively; Figure 5) and kink propagation rates (g_{oo} and g_{oa} at obtuse steps, g_{ao} and g_{aa} at acute steps, with $g_{oa} \approx g_{ao}$; Figure 5). Following the reasoning of Jordan et al.[39] for dissolution of magnesite, kinks with a slow propagation rate tend to bunch and to accumulate on a step when the propagation rate of the kink increasingly differs from the propagation rate of the faster kink at the step. This kink accumulation is eventually manifested morphologically by the observed change in step orientation. In turn, this means that the occurrence of kinks is inversely correlated with their reactivity.

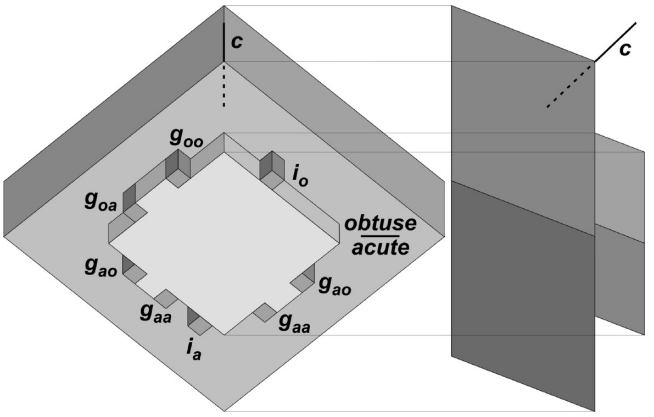

Figure 5. Schematic representation of a calcite crystal and a rhom-bus-shaped growth island on its (104) surface. At the growth island, the nomenclature of kink-formation sites i and kink sites g is given for the acute and obtuse steps.

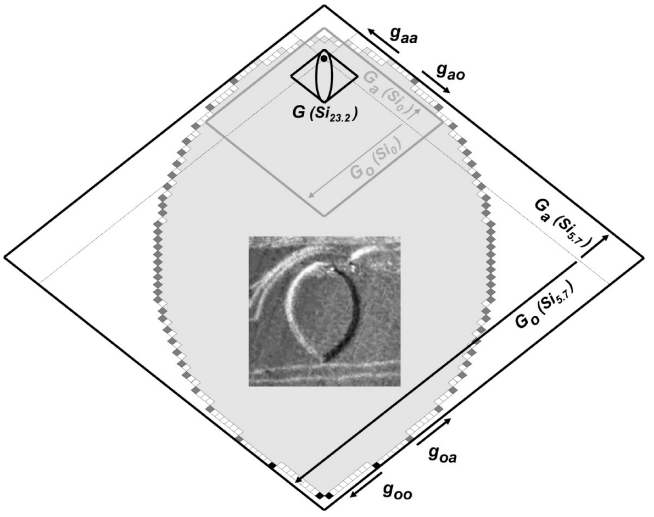

Figure 6. Scheme showing the shape of an growth island at βcalcite = 10 and [Si]tot = 5.7 ppm (the inset picture corresponds to Figure 4c). At the contour of the island the different step and kink sites are color-coded: goo (black); goa = gao (dark gray); gaa (pale gray); no kink site (blank). The island is enveloped by a rhomb. The size of the enveloping rhomb is a measure of the step velocity of acute steps (Ga) and obtuse (Go) with respect to the origin of the growth island (marked by the small black circle in the upper middle).

For comparison the rhomb envelope of the growth island at $\beta_{calcite}$ = 10 and $[Si]_{tot}$ = 0 (dark gray; labeled with the step velocities Go(Si0) and Ga(Si0)) as well as the ellipse growth island and its rhomb envelope at βcalcite = 10 and [Si]tot = 23.2 (black; labeled G(Si23.2)) have been inserted. The size of the growth islands and rhombuses is scaled to the respective step velocity.

Figure 6 shows the occurrence of kinks along the steps at $\beta_{calcite}$ = 10 and $[Si]_{tot}$ = 5.7 ≈ $[Si]_{p\ max}$. Judging by this scheme, g_{oa} kinks are the least reactive kink sites and there-fore the least promoted kink sites. However, it should be noted that since straight steps may also have a certain kink density, the model in Figure 6 tends to underestimate the density of goo and gaa kinks to some degree.

Increasing the silicic acid concentration to values .$Si_{p\ max}$ makes a small difference in the step morphology. Figure 4d taken at $[Si]_{tot}$=23.2 ppm reveals islands with an increased elongation and rounded obtuse/obtuse junctions. Thus, in the inhibition regime, g_{oa} kinks still are the least reactive kinks and, therefore, the most inhibited kinks - although all kinks around the entire ellipse have to be strongly inhibited to achieve such an overall reduction in step speed, as can be seen clearly in Figure 6. Finally, it is important to note that ellipses with the major axis along [421] are not a growth pattern generated exclusively by silicic acids as promoters or inhibitors but have also been observed on calcite (104) surfaces with, for example, Mg^{2+} as inhibitor.[16]

Conclusions

The bimodal polymerization state of silicic acids causes bimodal effects on step velocity: while polysilicic acids en-hance two-dimensional nucleation solely, mono- and oligo-meric silicic acids have a bimodal promoter/inhibitor effect. Therefore, silicic acids are extremely well qualified to control calcite growth kinetics.

Despite the multilevel bimodality of silicic acids, their effect on the morphology of growing calcite (104) surface is almost identical to that observed for the case of some small cationic inhibitors (e.g., Mg^{2+}). This strongly supports the idea of a general morphological convergence: a huge number of var-ious additives are related to a small number of different morphological patterns. This convergence marks a general limit of the chemical control in biological morphogenesis. The results presented in this paper demonstrate that the bimodal promoter/inhibitor effect of additives is not an exclusive property of large organic ligands such as proteins but is also an effect of inorganic molecules. If coupled with physical control mechanisms (such as templates), this strong kinetic effect can still be a very powerful tool for engineered crystal growth.

Finally, it is interesting to note that silicic acids are used by some organisms in biosynthetic processes. Therefore, silicic acids and silica may have a dual function as a biomineral constituent and as a powerful control agent for the formation of the important biomineral calcite.

Acknowledgment. This work was supported by the Spanish Ministry of Education and Science (Project No. HA2006-0022), by the Universidad Complutense-Comunidad de Madrid (Grant No. 910148-Superficies Minerales), by the DAAD (PPP-Programm "Acciones Integradas Hispano-Alemanas" D/06/12810), and by the Deutsche Forschungsgemeinschaft (DFG). The Centro de Microscopia (UCM) is acknowledged for kindly providing access to AFM. The manuscript has been improved by the helpful comments of Andrew G. Stack and four anonymous reviewers.

References

(1) Meldrum, F. C.; Colfen, H. Chem. Rev. 2008, 108, 4332–4432.
(2) Skinner, H. C. W. Min. Mag. 2005, 65, 621–641.
(3) Mann, S. Biomineralization; Oxford University Press: Oxford, 2001.(4) Gutjahr, A.; Dabringhaus, H.; Lacmann, R. J. Cryst. Growth 1996, 158, 310–315.
(5) Meldrum, F. C.; Hyde, S. T. J. Cryst. Growth 2001, 231, 544–558.(6) Fern´andez-Dı´az, L.; Astilleros, J. M.; Pina, C. M. Chem. Geol. 2006, 225, 314–321.

(7) Westin, K.-J.; Rasmuson, ° A.C. J. Colloid Interface Sci. 2005, 282, 359–369.

(8) Elhadj, S.; Salter, E. A.; Wierzbicki, A.; De Yoreo, J. J.; Han, N.; Dove, P. M. Cryst. Growth Des. 2006, 6, 197–201.

(9) Fu, G.; Qiu, S. R.; Orme, C. A.; Morse, D. E.; De Yoreo, J. J. Adv. Mater. 2005, 17, 2678–2683.

(10) Yang, M.; Stipp, S. L. S.; Harding, J. Cryst. Growth Des. 2008, 8, 4066–4074.

(11) Yu, S. H.; Colfen, H. J. Mater. Chem. 2004, 14, 2124–2147.

(12) Orme, C. A.; Noy, A.; Wierzbicki, A.; McBride, M. T.; Grantham, M.; T e n g , H . H . ; D o v e , P . M . ; D e Y o r e o , J . J . Nature 2001, 411, 7 7 5 –779.(13) Astilleros, J. M.; Pina, C. M.; Fern´andez-Dı´az, L.; Putnis, A. Geochim. Cosmochim. Acta 2000, 64, 2965–2972.

(14) Astilleros, J. M.; Pina, C. M.; Fern´andez-Dı´az, L.; Putnis, A. Geochim. Cosmochim. Acta 2002, 66, 3177–3189.

(15) Wasylenki, L. E.; Dove, P. M.; Wilson, D. S.; De Yoreo, J. J. Geochim. Cosmochim. Acta 2005, 69, 3017–3027.

(16) Davis, K. J.; Dove, P. M.; Wasylenki, L. E.; De Yoreo, J. J. Am. Mineral. 2004, 89, 714–720.

(17) Elhadj, S.; De Yoreo, J. J.; Hoyer, J. R.; Dove, P. M. Proc. Natl. Acad. Sci. U.S.A. 2006, 103, 19237–19242.

(18) Kim, I. W.; Darragh, M. R.; Orme, C.; Evans, J. S. Cryst. Growth Des. 2006, 6, 5 –10.

(19) Sangwal, K. Additives and Crystallization Processes; Wiley: New York, 2007.

(20) Vavouraki, A. I.; Putnis, C. V.; Putnis, A.; Koutsoukos, P. G. Chem. Geol. 2008, 253, 243–251.

(21) Williams, R. J. P. Introduction to silicon chemistry and biochemistry. In Silicon Biochemistry - Ciba Foundation Symposium 121; Evered, D., O'Connor, M., Eds.; Wiley: Chichester, 1986, pp 24-39.(22) Tarutani, T. Anal. Sci. 1989, 5, 245–252.

(23) Farmer, V. C. Sources and speciation of aluminium and silicon in natural waters. In Silicon Biochemistry - Ciba Foundation Sym-posium 121, Evered, D.; O'Connor, M., Eds.; Wiley: Chichester, 1986, pp 4-23.

(24) Imai, H.; Terada, T.; Yamabi, S. Chem. Commun. 2003, 484–485.(25) Lakshminarayanan, R.; Valiyaveettil, S. Cryst. Growth Des. 2003, 3, 6 1 1 –614.

(26) Garcı´a-Ruiz, J. M. Geology 1998, 6, 843–846.

(27) Garcı´a-Ruiz, J. M.; Hyde, S. T.; Carnerup, A. M.; Christy, A. G.; Van Kranendonk, M. J.; Welham, N. J. Science 2003, 302, 1194–1197.

(28) Garcı´a-Ruiz, J. M.; Melero-Garcı´a, E.; Hyde, S. T. Science 2009, 323, 362–365.

(29) Jordan, G.; Rammensee, W. Geochim. Cosmochim. Acta 1998, 62, 941–947.

(30) Jordan, G.; Pokrovsky, O. S.; Guichet, X.; Schmahl, W. W. Chem. Geol. 2007, 242, 487–499.

(31) Parkhurst, D. L.; Appelo, C. A. J. User's guide to PHREEQC (version 2). A computer program for speciation, batch-reaction, one-dimensional transport, and inverse geochemical calculations: US Geological Survey Water-Resources Investigations Report 99-4259, 2000; p 312.

(32) Crerar, D. A.; Axtmann, E. V. Geochim. Cosmochim. Acta 1981, 45, 1259–1266.

(33) Nielsen, A. E. J. Cryst. Growth 1984, 67, 289–310.

(34) Cabrera, N.; Vermilyea, D. A. The growth of crystal from solution. In Doremus, R. H., Roberts B. W., Turnbull, D., Eds.; Growth and Perfection of Crystals; London: Chapman & Hall, 1958; pp 393-410.

(35) Voronkov, V. V.; Rashkovich, L. N. Sov. Phys. Crystallogr. 1992, 37, 559–570.

(36) Voronkov, V. V.; Rashkovich, L. N. J. Cryst. Growth 1994, 144, 107–115.

(37) van Enckevort, W. J. P.; van den Berg, C. J. F.; Kreuwel, K. B. G.; Derksen, A. J.; Couto, M. S. J. Cryst. Growth 1996, 166, 156–161.(38) Davis, K. J.; Dove, P. M.; De Yoreo, J. J. Science 2000, 290, 1134–1137.

(39) Jordan, G.; Higgins, S. R.; Eggleston, C. M.; Knauss, K. G.; Schmahl, W. W. Geochim. Cosmochim. Acta 2001, 65, 4257–4266.